Design and Performance Analysis of Three Phase Line Start Synchronous Reluctance Motor Using Finite Element Analysis

Mandar Chaudhari[1], Anandita Chowdhury[2]

[1]Department of Electrical Engineering, Sardar Vallabhbhai National Institute of Technology, Surat, Gujarat, India (mandar.chaudhari@rediffmail.com) ORCID 0000-0002-7442-8195
[2]Department of Electrical Engineering, Sardar Vallabhbhai National Institute of Technology, Surat, Gujarat, India (ac@eed.svnit.ac.in) ORCID 0000-0001-8653-6639

Abstract

Three-phase Induction Motors (TPIM) are prevalent in industrial applications due to their numerous advantages. However, TPIM has comparatively lower efficiency than modern motor technologies like permanent magnet synchronous motor(PMSM), synchronous reluctance motor(SynRM), or switched reluctance motor(SRM). The expensive rare earth material and the inability of line starting operation discourage the replacement of TPIM with these modern energy-efficient motors. This research proposes a novel conversion of TPIM into Line Start SynRM (LS-SynRM) to cause a cost-effective and compatible performance solution. The proposed design modifications are carried out on the existing 0.5HP TPIM rotor and analyzed using finite element analysis (FEA) software. The parametric analysis determines optimum barrier parameters such as barrier end width, barrier position, barrier width, and rib width. The considerable effect of barrier dimensions on motor performance is evident from the analysis.

Author Keywords. barrier; efficiency; finite element analysis; line start; parametric analysis; synchronous reluctance motor; three-phase induction motor.

Type: Research Article

1. Introduction

The share of electricity utilization by industrial drives and motors is nearly 40% of world electrical power generation. Almost 70% of industrial power consumption is due to electric motors [Aníbal T. de Almeida et al.2014] used in the industries. Climate change around the globe urges new environment-friendly, energy-efficient motor technologies.

The three-phase induction motor (TPIM) technology has predominantly been focused so far due to its simple structure, low cost, and low maintenance requirement. However, a rotor cage claims power losses (about 20% of total losses) which leads to a temperature rise of the rotor [Aníbal T. de Almeida et al.2014]. Therefore, to deal with the global warming challenges, energy-efficient motors such as Permanent Magnet Synchronous Motors (PMSM), Switched Reluctance Motors (SRM), and Synchronous Reluctance Motors (SynRM) are recommended.

The addition of active material in A. G. Yetgin et al.2014 and Carlos Verucch et al. 2017, such as slits in the stator and rotor structure and magnetic wedges in the slots, improves the efficiency of the induction motor up to 1.5%. However, it hampers the starting performance. Using nanomaterial in the winding significantly reduces the joules losses [Lieutenant J., Ganesan, et al. 2013] at the cost of increased capital. Some research studies suggest optimized

designs of the motor structures to avoid the need for active materials and advanced materials that lead to higher costs [Pritish Kumar et al. 2020]. Aluminum cast cage rotors are light and economical compared with die-casted copper cage rotors. However, the copper cage rotors perform better. It encourages the machine makers to opt for copper cage rotors for higher-end applications [Mallard V et al. 2019 and Zhang, Q et al. 2018].

Although there have been numerous attempts in the literature to address efficiency improvements of induction motors, modern motor technologies like PMSMs, SRMs, and SynRMs are also under consideration by many research studies. The parallel research with these new technologies mainly aims to replace inefficient three-phase induction motors. The efficient operation, high power, torque density, and broader operating speed range make PMSMs popular [Kong Y et al. 2020]. However, the volatile market price added with the need for high-density permanent magnets (PM) and its demagnetization issues diverted the attention of researchers towards PM-free motors [Pellegrino et al. 2016]. SRMs and SynRMs avoid the rotor cage bars and PMs. They have many superior features like high efficiency, simple and rugged motor structure, and low cost.

Despite these features, the line starting ability of these motors has been a serious concern. These motors demand an expensive and sophisticated converter. The direct online operation of SRM with a simple rectifier circuit results in considerable performance degradation [K. Vijayakumar et al.2008 and Manuel Pereira et al. 2019 and Yasuei Yoneoka et al. 2011].

The study by Infineon, a motor manufacturer [Cimens et al. 2019], compared traditional IMs with SynRM to claim SynRM as an energy-efficient motor. The original research in [J. K. Kostko. 1923] proposes novel rotor geometry for enhanced performance. During the last two decades, the researchers have been focusing line starting ability of SynRM to make it more versatile like IMs. The effect of barrier and its shape, insertion of small PM sections in the barrier, on the performance of Line Start SynRM (LS-SynRM), has been addressed in [Samad et al. 2015]. The rotor parameters optimization has been proposed in [Alessandro et al. 2019] to improve line starting ability and steady-state performance. The study proposed in [Hyunwoo Kim et al. 2020] uses a hybrid combination of permanent magnets and SynRM to boost performance. These types of motors are labeled PM-assisted SynRM. Even though the optimum dimensioning of barrier and PMs has not been carried out by [Hyunwoo et al. 2020], the PM-assisted LS-SynRM has shown efficiency improvements. In [Nezih Gokhan et al. 2019], the designs and prototypes of three differently rated IMs compared with compatible LS-SynRMs. Further studies on LS-SynRM reported in Boroujeni et al. 2011, and Liu et al. 2017 suggested LS-SynRM as a better substitute for induction motor (IM) considering its operational advantages.

However, in the pursuit of better performance by LS-SynRM, a new rotor is needed that demands an assembly line set up for rotor manufacturing. It leads to high capital requirements. Hence this research proposes a viable and inexpensive solution to the problem. It suggests a novel approach to existing TPIM rotor structure modification. It alters TPIM to LS-SynRM, which remains overlooked in the literature. This remodeling of the rotor exhibits negligible cage losses at synchronism that leads to better efficiency. The authors in [Mandar et al. 2021] presented a similar analysis for single-phase LS-SynRM.

The governing equations of the three-phase line start SynRM given in Section 2 of the paper. Section 3 describes the proposed design procedure, and the simulation model of the three-phase line start SynRM. Section 4 addresses the benchmark three-phase 0.5HP induction motor simulation in Ansys Maxwell™ for rated load condition. Section 5 discusses the FE-based

sensitivity analysis results of rotor structures for different parameters. Conclusions are reported in Section 6.

2. Three Phase Line Start Synchronous Reluctance Motor

In line start SynRM, the cage develops the starting torque and synchronism achieved by the reluctance torque caused due to saliency created by cut-out and barrier [M. Gamba et al. 2015].
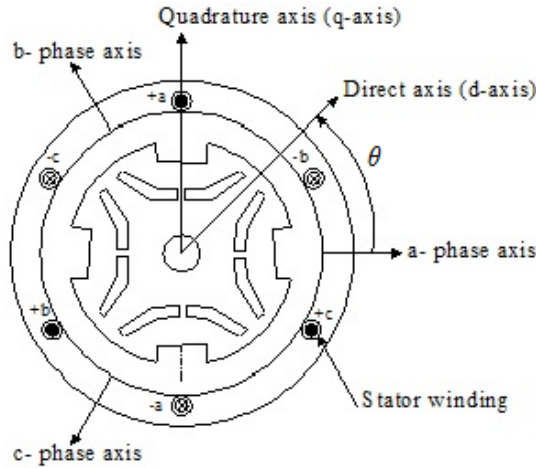

Figure 1: Model of Three phase LS-SynRM

The equations concerning (**Figure 1**) in rotor reference frame for three phase line start synchronous reluctance motor are given by (1)-(10) [Nicola Bianchi. 2005], where, vd, vq, id, iq and ψd, ψq are the d- axis and q-axis voltages, currents and flux linkages respectively. Rs is the stator resistance per phase and ω is the electrical speed. Voltage and current equations in dq- axis are represented by equations (1)-(4).

$$v_d = R_s i_d + \frac{d\psi_d}{dt} + \omega\psi_q \tag{1}$$

$$v_q = R_s i_q + \frac{d\psi_q}{dt} + \omega\psi_d \tag{2}$$

$$i_d = \frac{2}{3}\left[i_a cos\theta + i_b cos(\theta - \frac{2\pi}{3}) + i_c cos(\theta - \frac{4\pi}{3}) \right] \tag{3}$$

$$i_q = \frac{-2}{3}\left[i_a sin\theta + i_b sin(\theta - \frac{2\pi}{3}) + i_c sin(\theta - \frac{4\pi}{3}) \right] \tag{4}$$

where, ia, ib, and ic are stator currents of phase a, phase b, and phase c, respectively. θ is the electrical angle between showing the position of the d-axis with respect to the a- phase axis.

The dq- axis flux linkages are demonstrated by equations (5) and (6)

$$\psi_d = \frac{2}{3}\left[\psi_a cos\theta + \psi_b cos(\theta - \frac{2\pi}{3}) + \psi_c cos(\theta - \frac{4\pi}{3}) \right] \tag{5}$$

$$\psi_q = \frac{-2}{3}\left[\psi_a sin\theta + \psi_b sin(\theta - \frac{2\pi}{3}) + \psi_c sin(\theta - \frac{4\pi}{3}) \right] \tag{6}$$

After computing flux linkages and currents, the direct and quadrature axis inductances are calculated by equations (7) and (8).

$$L_d = \frac{\psi d}{i_d} \tag{7}$$

$$L_q = \frac{\psi q}{i_q} \tag{8}$$

The electromagnetic torque developed by line start SynRM is expressed by following equations.

$$T_e = T_{cage} + T_{rel} \tag{9}$$

$$T_e = \frac{m}{2}\frac{p}{2}\frac{L_m}{L_r}L_m i_d + \frac{m}{2}\frac{p}{2}\left(L_d - L_q\right)i_d i_q \tag{10}$$

where, Tcage and Trel are cage and reluctance torque, respectively, m is the number of phases, where the value of m is 3, p is the number of poles, Lm and Lr are the magnetizing and rotor inductances, respectively.

The mechanical power developed is calculated as equation (11), where ω is the angular speed in rad/sec.

$$P_{mech} = T_e \times \omega \tag{11}$$

Total losses are determined by adding core losses (Pcore), copper losses (Pcu), and extra losses. Extra losses are friction windage and stray losses. Friction windage losses are taken as 1.2% of output power, and stray losses are considered to be 1% [Boldea. 2020].

The electrical power input is then determined as

$$P_{elect} = P_{mech} + P_{core} + P_{cu} + Extra\ Loss \tag{12}$$

Finally steady state efficiency, η is calculated as equation (13)

$$\eta = \frac{P_{mech}}{P_{elect}} \tag{13}$$

3. Proposed Design Procedure for Three Phase LS-SynRM

This section describes detailed design procedures and design parameters under consideration.

3.1. Design Method

The proposed converted three-phase LS-SynRM must conform to the two significant tests. It must have line starting and synchronization at full load, in addition to the high efficiency at rated load. For proposed LS-SynRM stator structure and winding are kept the same as that of the three-phase induction motor. The structural modifications in cut-out and barrier are carried in the rotor only. The cut-out and barrier affect the reluctance torque developed due to saliency caused by the same. However, it has also been determined in Mandar et al. 2021 that mere cut-out on the rotor does not lead to significant performance improvement. Hence,

the work focuses on barrier design, keeping the same cut-out dimension. A simple line angled barrier is introduced in the rotor and analyzed. Barrier parameters such as barrier end width (Bew), barrier position (Bpos), barrier width (Bw) and, rib width (Rw) are taken for parametric sensitivity analysis and described in (**Table 1**). A Total of 25 models are created and analyzed for the performance of the proposed LS-SynRM.

Number of barriers	Barrier end width, B_{ew}	Position of barrier, B_{pos}	Width of barrier, B_w	Rib width, R_w
				0
	3mm	12mm	2mm	0.25mm
One barrier	2.5mm	14mm	3mm	0.5mm
	2mm	15mm	4mm	0.75mm
	1.5mm	16mm	5mm	1mm
Number of barriers	Barrier end width, Bew	Position of barrier, Bpos	Width of barrier, Bw	Rib width, Rw
				0
	3mm	12mm	2mm	0.25mm
One barrier	2.5mm	14mm	3mm	0.5mm
	2mm	15mm	4mm	0.75mm
	1.5mm	16mm	5mm	1mm

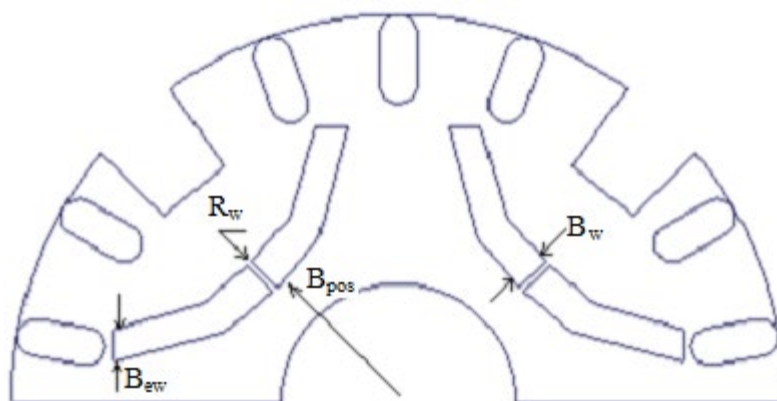**Table 1:** Design parameters under consideration

Figure 2: Rotor structure with barrier parameters

The proposed modified rotor is as shown in (**Figure 2**). Also, the summarized design procedure in the chart is described in (**Figure 5**).

3.2. Simulation Model

Magnetic equivalent circuit analysis and finite element analysis (FEA)[Wang X et al. 2006 and Lee et al. 2009] are the two general approaches for designing electromagnetic components. The magnetic equivalent circuit analysis approach uses the modeling of the magnetic circuit path with ampere-turns. Later, the network theory techniques are applied to solve the circuit. The rotor structure of SynRM is complex to analyze with the magnetic circuit analysis technique. In such cases, the finite element analysis approach is suitable for design [Lee B et al. 2012 and Li N et al. 2019]. The FEA accurately solves complex electromagnetic structures. It can also take into account time-varying fields and non-homogeneous materials. Also, flux distribution affected by structural modifications and material is taken into account precisely by FEA.

FEA divides the domain into finite elements and solves it by Maxwells' equations. It considers triangle elements for 2D analysis and tetrahedron elements for 3D analysis, as shown in (**Figure 3**a) and (**Figure 3**b), called mesh. The accuracy of the solution is highly dependent on the number of meshes in the region. The analysis region has constrained by the set boundaries for the definite result [Nicola Bianchi. 2005].


a) Two dimensional Finite element-Triangle   b) Three dimensional finite element-Tetrahedron

Figure 3: Finite element for 2D and 3D

FEA follows, in general, the step by step procedure to solve the electromagnetic field problems-

1. Geometrical modeling

2. Assigning material properties to each part of the model

3. Meshing

4. Assigning boundary conditions

5. Solver setup setting

6. Analysis

7. Solution

The geometrical model of the three-phase induction motor was created in ANSYS Maxwell FE software and then assigned with the materials. The magnetic cores and cage conductors respectively use JFE_Steel_50JN1000 and aluminum. For mesh generation, it uses length-based mesh and adaptive meshing techniques. The mesh models for TPIM and proposed LS-SynRM are shown in (**Figure 4**a) and (**Figure 4**4b), respectively. The number of mesh for TPIM is 4024 and for LS-SynRM is 4196.
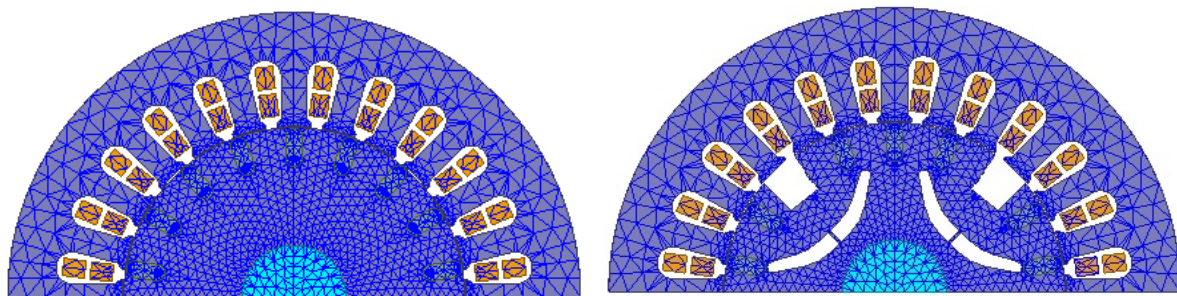
a) TPIM   b) Three phase LS-SynRM
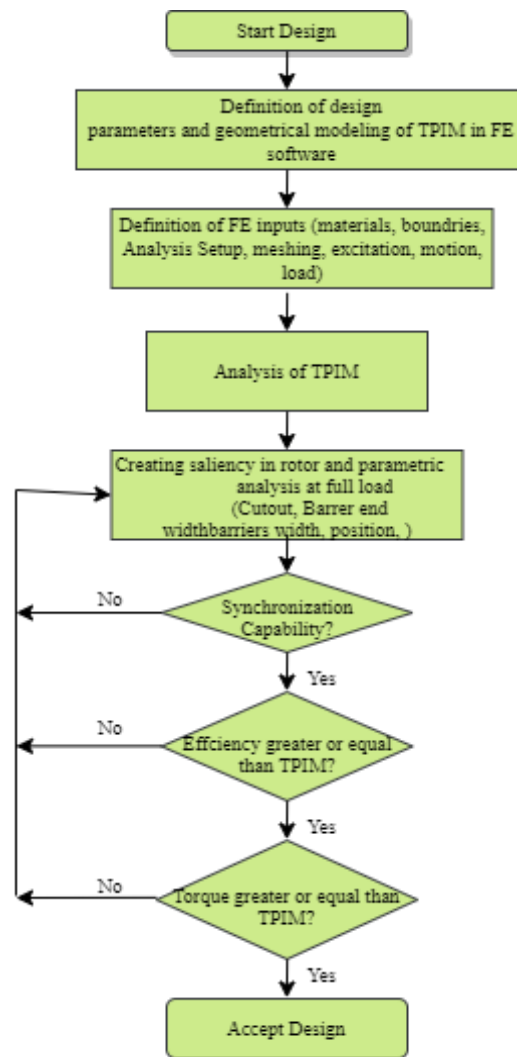
Figure 4: Mesh Models

Figure 5: Systematic design procedure for three phase LS-SynRM

Maxwell's model of the motors is excited with an external coupled circuit. The supply voltage to the motor kept three-phase 415V, and the time step given to analyze setup is 20ms. A software model of TPIM analyzes motor geometry and excitation for rated load conditions. Further, the cutout and barrier were introduced and analyzed for the rated load. The analysis accounts for synchronizing ability, efficiency, and torque. However, the non-compliance of the results repeats the design procedure.

4. Benchmark Motor Performance Analysis

A 0.5Hp, 415V, 50 Hz, three induction motor with geometrical parameters given in Table 2 is taken as a benchmark motor and analyzed.

Parameter	Dimension
Stator outer diameter	105mm
Bore Diameter	63mm
Stack Length	75mm
Air gap length	0.35mm
Rotor outside diameter	62.65mm
Number of stator slots	24
Number of rotor slots	18
Number of poles	4

Table 2: Three phase induction motor geometrical parameters

The motor rotor is aluminum die-casted with stainless steel shaft. (**Figure 6**) shows the geometry of the three-phase induction motor. The stator winding resistance per phase is 13.64 ohm. The moment of inertia was 0.00103 kg- m2.
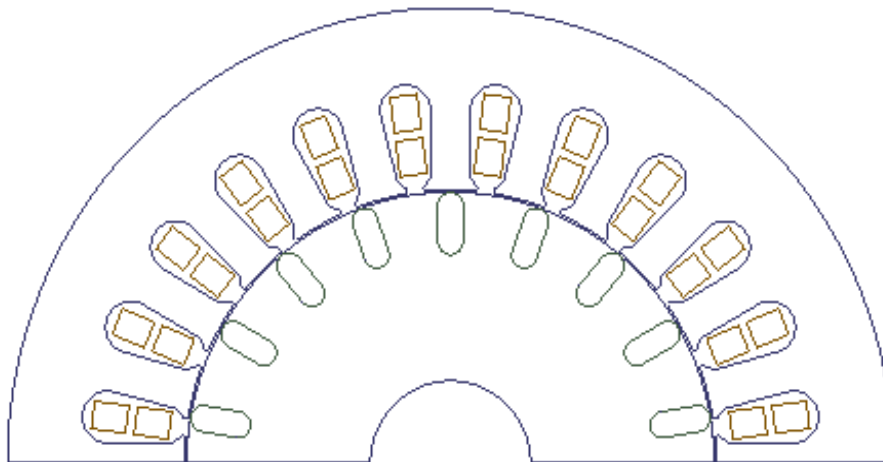

Figure 6: Ansys Maxwell geometry of three phase induction motor

Geometrical dimensions and winding distribution data are taken from the practical motor and simulated in FEM software. Transient 2D simulation results of a three-phase induction motor with a rated load are as shown in (**Figure 7**a) to (**Figure 7**d). Core losses, stator copper losses, and rotor copper losses, respectively, were determined as 11.22W, 51.37W, and 23.8W. Additional losses are 8.5W. The output mechanical power developed is 383.73W with a rated torque of 2.6N-m and a speed of 1410rpm. The calculated full load efficiency of TPIM is 80.1%.
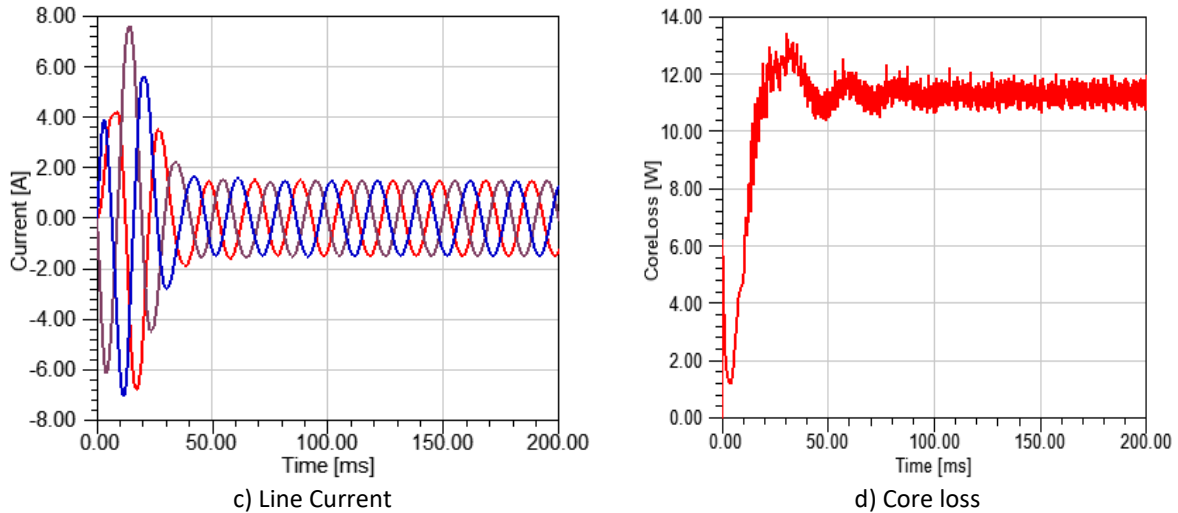

a) Torque

b) Speed

c) Line Current   d) Core loss
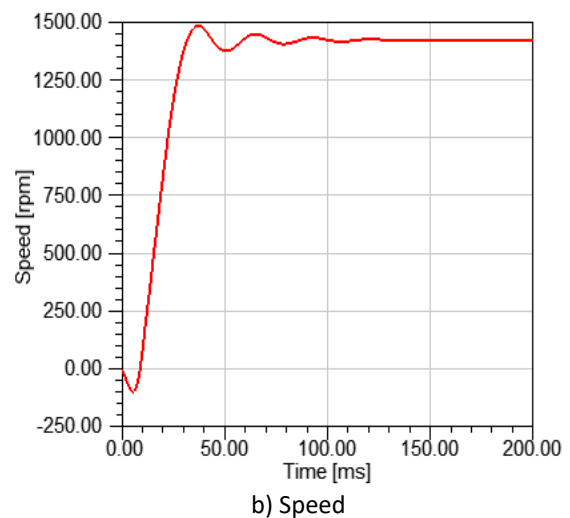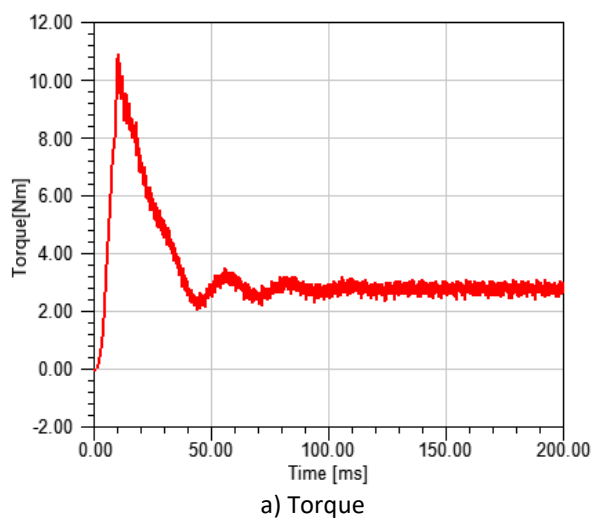
Figure 7: Performance results of TPIM

5. Results And Discussions

The three-phase line start synchronous reluctance motor has been analyzed to investigate the performance through barrier design. The proposed design method analyzes the effect of barrier parameters like barrier position, width, end width, and rib width. The analysis uses barrier variations to examine synchronizing ability, efficiency, and torque performance.

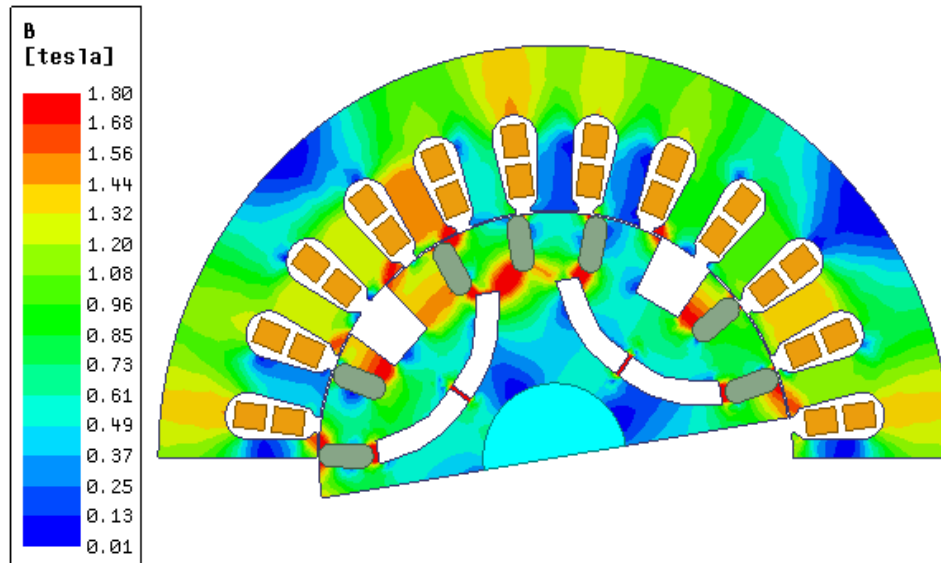### 5.1. Parametric Analysis on Barrier End-width (Bew)

The study investigates optimized barrier dimensions through parametric analysis. The barrier end widths have varied from a maximum of 3mm to 1.5mm in steps of 0.5mm.

| B_{ew} (mm)	Torque (Nm)	P_{mech} (W)	P_{elect} (W)	P_{cu} (W)	P_{core} (W)	Extra loss (W)	Efficiency (%)	L_d/L_q
3.00	2.53	398.75	705.16	274.50	23.14	8.77	56.55	2.46
2.50	2.53	394.64	482.72	66.00	13.40	8.68	81.75	1.68
2.00	2.53	397.78	492.72	72.38	13.81	8.75	80.73	1.70
1.50	2.53	396.43	494.88	75.69	14.04	8.72	80.11	1.71

Table 3: Motor performance of variations in barrier end width

Table 3 describes the performance with a barrier position of 14mm and a barrier width of 3mm. It shows inferior results for the 3mm end width. However, the 2.5mm end width performance results in the highest efficiency of 81.75% among all the designated variations. It has also revealed that a further decrease in end width from 2.5mm exhibits poor performance due to increased losses. Moreover, the end width does not affect the developed torque of the motor.

The torque ripples for 2.5mm end width has been 11% and 19.6% less than 2mm and 1.5mm, respectively. The saliency ratio in terms of direct axis and quadrature axis inductance has a marginal effect for variations between 2.5mm to 1.5mm end width. However, identical barrier width and end width cause the highest saliency ratio. It is because the direct axis part of the rotor flux, in this case, is utilized adequately. Also, it is clear from (**Figure 8**a) and (**Figure 8**b) that the overcrowding of flux at 3mm end width leads to non-uniform flux distribution compared with 2.5mm.

a) Barrier end width 3mm
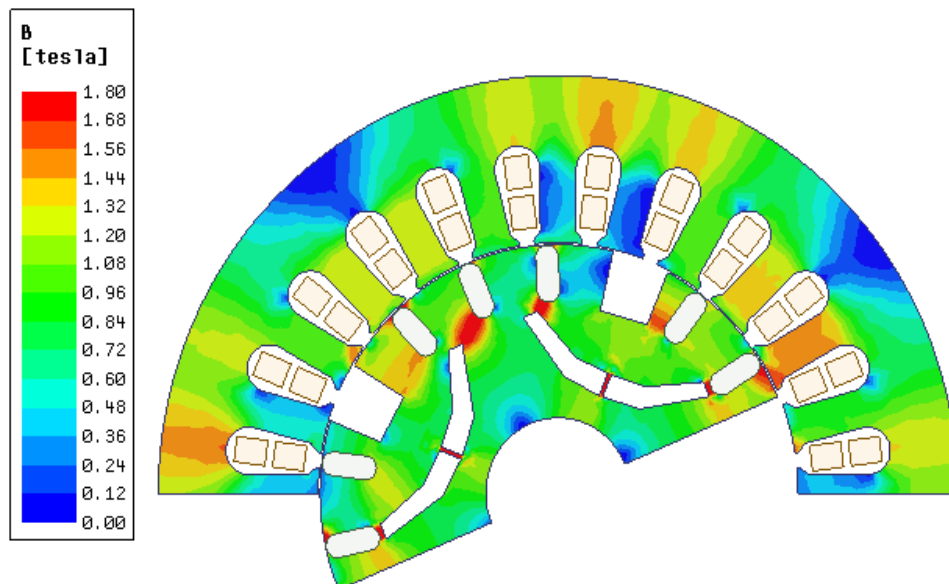
b) Barrier end width 2.5 mm

Figure 8: Flux density plots

5.2. Parametric Analysis on Rotor Barrier Position and Barrier Width

Different barrier positions and widths affect synchronizing ability and saliency ratio, and (**Table 4**) mentions the results. The synchronization capability of the investigated models for four different barrier widths at each of the prescribed barrier positions reports that nine models successfully synchronized among the sixteen models. However, none of the models at barrier position 12mm successfully synchronized. Moreover, the barrier position of 16mm at a width of 3mm leads to the highest saliency.

Position (mm)	Width (mm)	Synchronization	Ld/Lq
12.00	2.00	N0	2.51
	3.00	No	2.22
	4.00	No	2.70
	5.00	No	2.39
14.00	2.00	No	2.04
	3.00	Yes	1.69
	4.00	No	2.46
	5.00	No	2.44
15.00	2.00	Yes	2.41
	3.00	Yes	1.70
	4.00	Yes	1.73
	5.00	Yes	1.78
16.00	2.00	Yes	1.85
	3.00	Yes	1.86
	4.00	Yes	1.79
	5.00	Yes	1.63

Table 4: Effect of barrier position and width on the synchronizing ability and saliency ratio

The successfully synchronized nine models have further taken up for the performance analysis. It has been evident from the results, as given in (**Table 5**), that 14mm barrier position and 3mm barrier width result in the highest efficiency. Also, (**Table 6**) reports a detailed analysis of the total losses. Shifting the barrier away from the center of the shaft results in poor performance due to increased losses. It has also been observed that copper losses are the major contributor to the total losses. It is due to saturation in the rotor and subsequent increase in the current. Also, the reduced iron material in the proposed LS-SynRM rotor may increase the reactive power required to magnetize the LS-SynRM. However, the core losses at steady state are also affected by the barrier position and width, shown in (**Figure 9**a) to (**Figure 9**c). The core losses and the core loss harmonics increase as the barrier position shifts away from the center.

Position (mm)	Width (mm)	Torque (Nm)	P_{mech} (W)	P_{elect} (W)	Total Loss (W)	Efficiency (%)
14.00	3.00	2.53	394.64	482.72	88.08	81.75
15.00	2.00	2.51	394.25	498.77	104.52	79.04
	3.00	2.52	395.43	489.23	93.80	80.83
	4.00	2.53	397.46	491.11	93.65	80.93
	5.00	2.52	394.89	495.22	100.33	79.74
16.00	2.00	2.52	396.23	500.78	104.55	79.12
	3.00	2.52	396.01	495.50	99.49	79.92
	4.00	2.52	396.55	499.57	103.02	79.38
	5.00	2.52	395.30	515.89	120.59	76.62

Table 5: Motor performance of synchronized models

| Position (mm)	Width (mm)	P_{core} (W)	P_{core-S} (W)	P_{core-R} (W)	I_L (A)	P_{cu} (W)	Extra loss (W)
14.00	3.00	13.40	11.18	2.23	1.27	66.00	8.68
15.00	2.00	14.49	12.03	2.46	1.41	81.35	8.67
	3.00	13.80	11.50	2.30	1.32	71.30	8.70
	4.00	13.61	11.35	2.26	1.32	71.30	8.74
	5.00	13.71	11.39	2.32	1.38	77.93	8.69
16.00	2.00	14.48	12.04	2.44	1.41	81.35	8.72
	3.00	13.98	11.64	2.34	1.37	76.80	8.71
	4.00	14.09	11.71	2.38	1.40	80.20	8.72
	5.00	14.85	12.28	2.57	1.54	97.05	8.70

Table 6: Losses of synchronized models
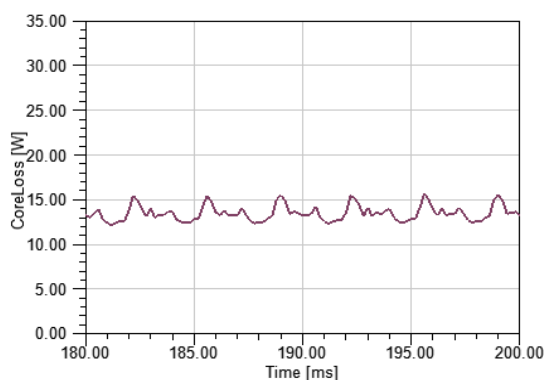
a) Barrier position 14mm and width 3mm
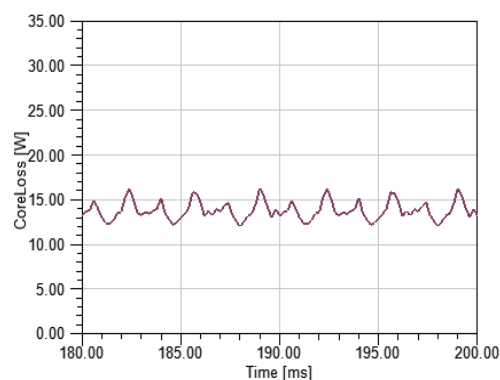
b) Barrier position 15mm and width 3mm
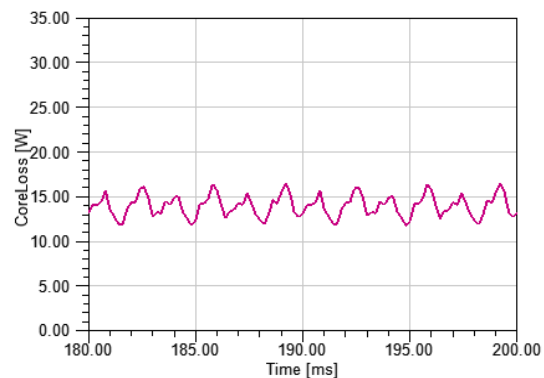
c) Barrier position 16mm and width 3mm

Figure 9: Core loss at steady-state for different barrier positions and barrier widths

The developed torque is found consistent for all the synchronized models. However, the stator mmf harmonics and rotor structure interaction result in torque ripples. The 17% lesser ripples for 14mm barrier position and 3mm width than that for 15mm and 16mm barrier positions at the width of 3mm were observed. It is also observed that as barrier width increases, the torque ripple reduces. Approximately, 40% reduction in torque ripple was noted as the width changed from 2mm to 5mm for barrier positions of 15mm and 16mm.

Considering the significance of the reluctance torque, the variation in barrier positions and widths has been investigated. (**Figure 10**) describes the reluctance torque developed by the

motor for different barrier positions. The barrier position of 16mm results in the highest reluctance torque (**Figure 10**c). It is approximately 20% more than that at 14mm and 15mm.
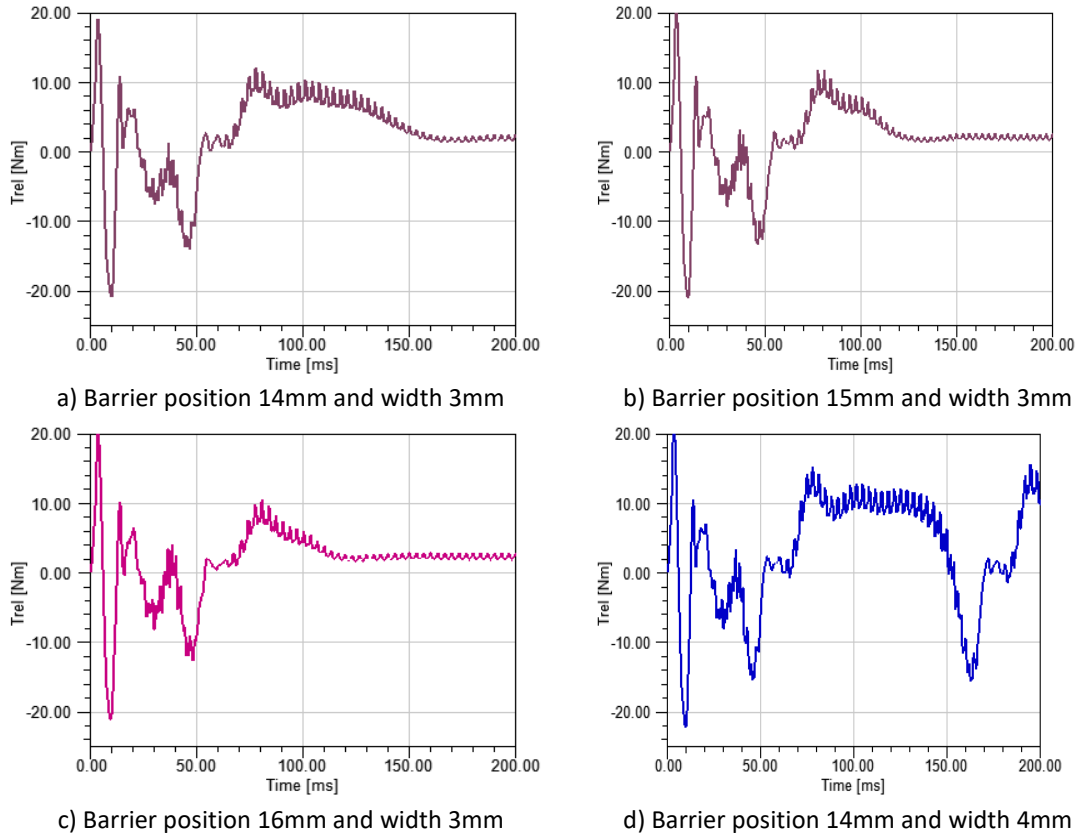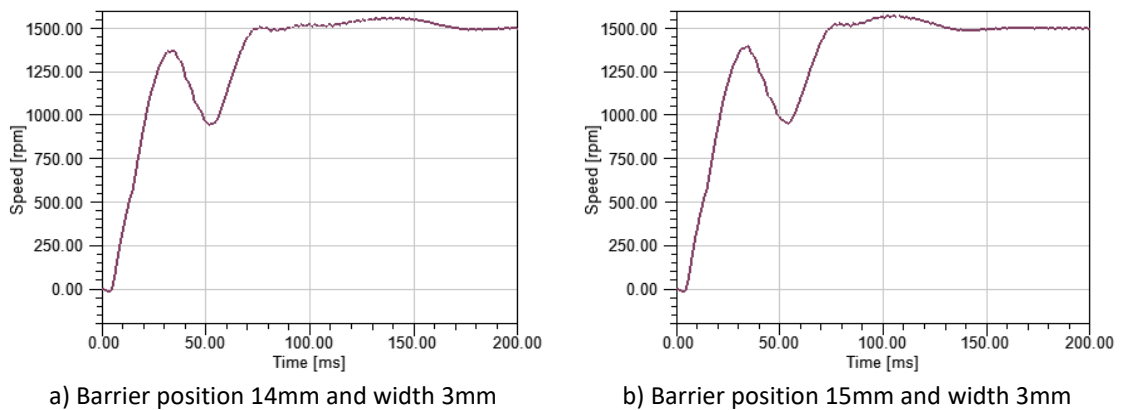

a) Barrier position 14mm and width 3mm

b) Barrier position 15mm and width 3mm

c) Barrier position 16mm and width 3mm

d) Barrier position 14mm and width 4mm

Figure 10: Reluctance torque

As observed from (**Figure 10**) and (**Figure 11**), the rotor attains synchronism in 170ms, 150ms, and 130ms for barrier positions of 14mm, 15mm, and 16mm, respectively. It indicates that 16mm barrier position yields better induction and reluctance torque. The model with a barrier position of 14mm and a width of 4mm does not synchronize due to insufficient reluctance torque, seen in (**Figure 11**d).
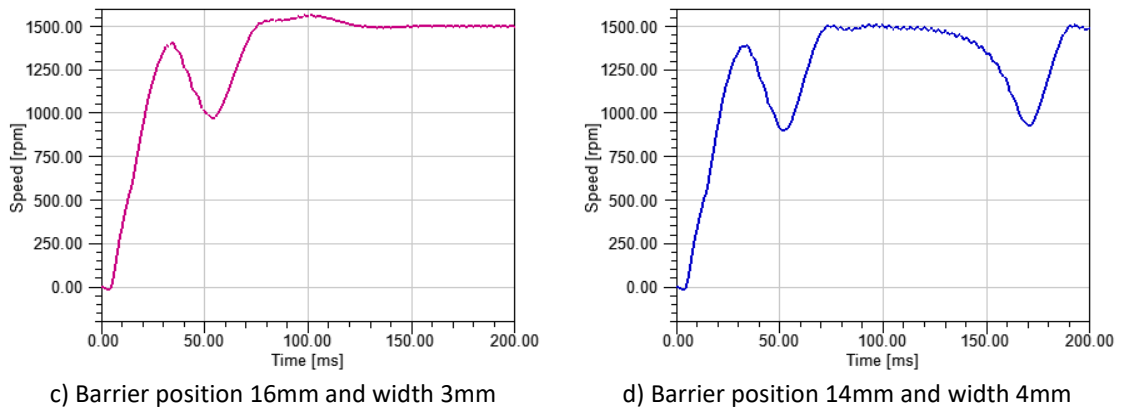

a) Barrier position 14mm and width 3mm

b) Barrier position 15mm and width 3mm

c) Barrier position 16mm and width 3mm   d) Barrier position 14mm and width 4mm

Figure 11: Speed plots for various barrier positions

The analysis of synchronizing ability, developed torque, and torque ripples are further taken forward to study the significant performance index as efficiency. The efficiency at various loading conditions for the barrier position of 14mm, 15mm, and 16mm for the width of 3mm was analyzed. (**Figure 12**) shows efficiency at different loading conditions, and the highest efficiency of 81.91 % was recorded at 75% of full load among all the investigated models. At 75% loading, the model with a 14mm barrier position is 1.01% and 2.08% more efficient than that barrier position of 15mm and 16mm, respectively. Speed plots for different loading conditions, as shown in (**Figure 13**), delivered maximum starting transients at no-load; however, it decreases as the load torque increases.
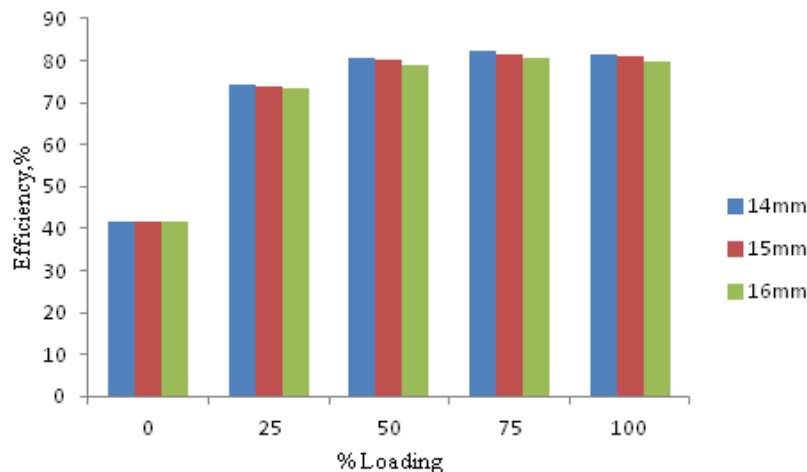

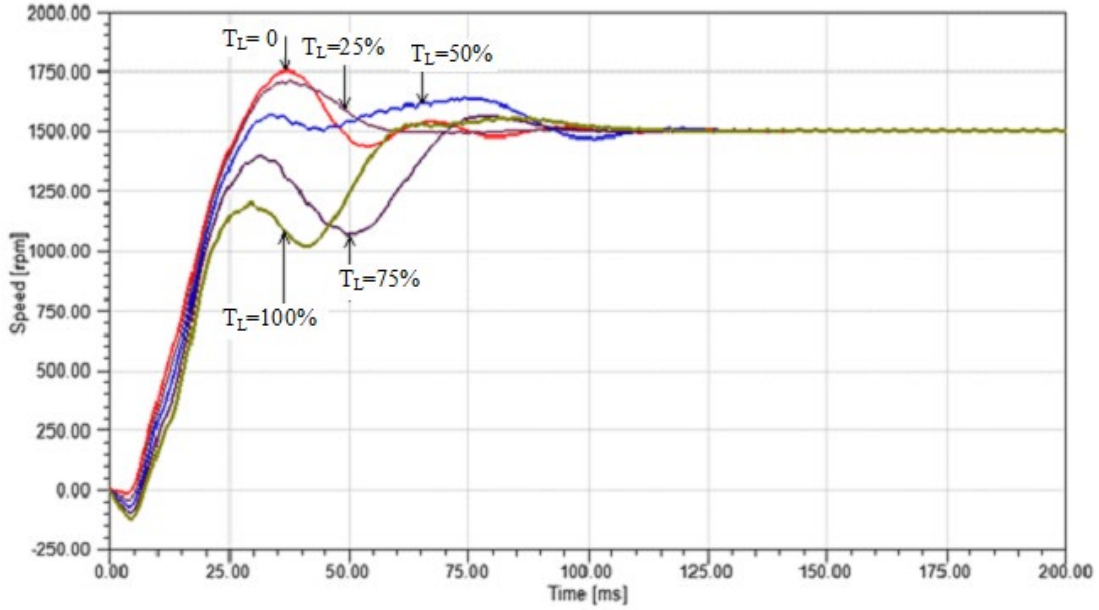**Figure 12:** Efficiency at various load condition

Figure 13: Speed at various load condition for barrier position of 14mm

5.3. Parametric Analysis on rib width

The rib is the iron part in the middle of the barrier, as seen in **Figure 2**. The larger the rib width more is the mechanical strength of the rotor. To investigate the effect of variation of rib width on the performance, rib width was varied from 0mm to 1.00mm in steps of 0.25mm as illustrated in (**Table 7**), keeping barrier position and width at 14mm and 3mm, respectively. The rib width of 0mm and 0.25mm motor does not yield synchronism. However, for the width of 0.5mm, and more, the efficiency decreases. Rib width of 0.5mm records the highest efficiency. The efficiency dropped by 1.34% for the increase in the rib width from 0.5mm to1.0mm. It is due to an 8% increase in copper losses and 3% in core losses. The increase in the rib width, however, affects the torque ripples. The torque ripple in the case of rib width of 0.75mm and 1mm is 3.84% and 11.53% more, respectively, compared to 0.5mm rib width.

Rib Width (mm)	P_{mech} (W)	P_{elect} (W)	P_{core-S} (W)	P_{core-R} (W)	I_L (A)	P_{cu} (W)	Extra loss (W)	Total loss (W)	Efficiency (%)
0.00									
0.25				Could Not Synchronize					
0.50	401.21	491.61	11.18	2.23	1.27	66.00	8.68	88.08	81.75
0.75	397.98	491.74	11.42	2.29	1.32	71.30	8.76	93.76	80.93
1.00	397.50	493.62	11.57	2.33	1.34	73.48	8.75	96.12	80.53

Table 7: The effect of rib width on the performance

5.4. Material Consumption

(**Table 8**) presents the comparison of materials in p.u for the TPIM and the proposed LS-SynRM. The proposed conversion to LS-SynRM claims 18% less active material than conventional TPIM. It will lead to an 18% reduction in the weight of the motor. However, the barrier in the rotor will also act as a ventilating duct resulting in better cooling of the rotor.

Material	TPIM	LS-SynRM
Magnetic Material (pu)	0.87	0.72
Conducting material(pu)	0.13	0.1
Total(pu)	1	0.82

Table 8: Consumption of material in p.u.

6. Conclusions

The research work presented in the paper addresses a viable and cost-effective design method for realizing LS-SynRM from the conventional TPIM. The performed analysis results in terms of barrier end width, barrier position, width, and rib width showcased the improved performance of LS-SynRM.

The parametric analysis taking into account barrier end width demonstrated that a model with an end width of 2.5mm has better efficiency and torque profile than the other designated models. It has been noted that the further decrease in the end width (below 2.5mm) leads to the rise in power losses and inferior performance. However, the end width variation does not affect the developed torque.

Further analysis of barrier position and its width variation demonstrated a significant influence on the overall motor performance. The investigations among the entire successfully synchronized model have outlined the optimum barrier position of 14mm from the center of the shaft with a barrier width of 3mm. The maximum efficiency noted, in this case, was 81.75 % which is 2.5 % higher than the average efficiency of the other analyzed models. However, the ripples in the torque were found 17% less in this case, compared to the other barrier positions. Moreover, it was seen that shifting the barrier away from the center of the shaft results in increased losses. The increase in barrier width reduces ripples at the cost of increased line current (IL) and subsequent losses. The time required to attain steady-state operation of the motor also depends on the barrier position. Farther the barrier from the shaft lesser the time required for successful synchronism.

The motor performance is also a function of rib width. The analysis of variation in the rib width has shown that the absence of rib width results in the non-synchronous operation of the motor. However, 0.5mm rib width earmarked maximum performance improvements. The proposed conversion of TPIM to LS-SynRM has proven 2% higher efficiency with reduced material requirements. However, introducing the barriers may also provide better cooling of the rotor. The proposed converted three-phase LS-SynRM can be suitable in low-power constant speed applications.

References

Almeida, Anibal T. de, Fernando J. T. E. Ferreira, and Ge Baoming. 2014. "Beyond Induction Motors—Technology Trends to Move Up Efficiency." *IEEE Transactions on Industry Applications* 50 (3): 2103–14. https://doi.org/10.1109/TIA.2013.2288425.

Bianchi, Nicola. 2017. *Electrical Machine Analysis Using Finite Elements*. 0 ed. CRC Press. https://doi.org/10.1201/9781315219295.

Boroujeni, S T, N Bianchi, and L Alberti. 2011. "Fast Estimation of Line-Start Reluctance Machine Parameters by Finite Element Analysis." *IEEE Transactions on Energy Conversion* 26 (1): 1–8. https://doi.org/10.1109/TEC.2010.2061851.

Boroujeni, Samad Taghipour, Mortaza Haghparast, and Nicola Bianchi. 2015. "Optimization of Flux Barriers of Line-Start Synchronous Reluctance Motors for Transient- and Steady-State

Operation." *Electric Power Components and Systems* 43 (5): 594–606. https://doi.org/10.1080/15325008.2014.984819.

Castagnini, Alessandro, Lucia Frosini, Michele Maggi, and Mattia Pinna. 2019. "Design and Test of a Novel Direct-On-Line Synchronous Reluctance Motor." In *2019 21st European Conference on Power Electronics and Applications (EPE '19 ECCE Europe)*, P.1-P.10. Genova, Italy: IEEE. https://doi.org/10.23919/EPE.2019.8915026.

Mandar, Chaudhari, Anandita Chowdhury, Gajanan Dhole. 2021. "Effect of Flux Barrier Shape on Performance of Single-Phase Line Start Synchronous Reluctance Motor Modified from Single Phase Induction Motor." *Electrica* 21 (3): 322–41. https://doi.org/10.5152/electrica.2021.20104.

Clemens, Muller and Ulrich, Schwarzer. 2019. *Handbook of Electric Machines: Motor Handbook*. Version 2.1 vols. Germany: Infineon Technologies.

Gamba, M., E. Armando, G. Pellegrino, A. Vagati, B. Janjic, and J. Schaab. 2015. "Line-Start Synchronous Reluctance Motors: Design Guidelines and Testing via Active Inertia Emulation." In *2015 IEEE Energy Conversion Congress and Exposition (ECCE)*, 4820–27. Montreal, QC, Canada: IEEE. https://doi.org/10.1109/ECCE.2015.7310340.

Ghosh, Pritish Kumar, Pradip Kumar Sadhu, Raju Basak, and Amarnath Sanyal. 2020. "Energy Efficient Design of Three Phase Induction Motor by Water Cycle Algorithm." *Ain Shams Engineering Journal* 11 (4): 1139–47. https://doi.org/10.1016/j.asej.2020.01.017.

Kim, Hyunwoo, Yeji Park, Huai-Cong Liu, Pil-Wan Han, and Ju Lee. 2020. "Study on Line-Start Permanent Magnet Assistance Synchronous Reluctance Motor for Improving Efficiency and Power Factor." *Energies* 13 (2): 384. https://doi.org/10.3390/en13020384.

Kong, Yong, Mingyao Lin, and Lun Jia. 2020. "A Novel High Power Density Permanent-Magnet Synchronous Machine With Wide Speed Range." *IEEE Transactions on Magnetics* 56 (2): 1–6. https://doi.org/10.1109/TMAG.2019.2947611.

Kostko, J. K. 1923. "Polyphase Reaction Synchronous Motors." *Journal of the American Institute of Electrical Engineers* 42 (11): 1162–68. https://doi.org/10.1109/JoAIEE.1923.6591529.

Lee, Byeong-Hwa, Jung-Pyo Hong, and Jung-Ho Lee. 2012. "Optimum Design Criteria for Maximum Torque and Efficiency of a Line-Start Permanent-Magnet Motor Using Response Surface Methodology and Finite Element Method." *IEEE Transactions on Magnetics* 48 (2): 863–66. https://doi.org/10.1109/TMAG.2011.2175207.

Li, Nian, Jianguo Zhu, Mingyao Lin, Gongde Yang, Yong Kong, and Li Hao. 2019. "Analysis of Axial Field Flux-Switching Memory Machine Based on 3-D Magnetic Equivalent Circuit Network Considering Magnetic Hysteresis." *IEEE Transactions on Magnetics* 55 (6): 1–4. https://doi.org/10.1109/TMAG.2019.2900368.

Liu, Huai-Cong, Hyun-Seok Hong, Sooyoung Cho, Ju Lee, and Chang-Sung Jin. 2017. "Bubbles and Blisters Impact on Diecasting Cage to the Designs and Operations of Line-Start Synchronous Reluctance Motors." *IEEE Transactions on Magnetics* 53 (6): 1–4. https://doi.org/10.1109/TMAG.2017.2663109.

Mallard, Vincent, Guillaume Parent, Cristian Demian, Jean-Francois Brudny, and Aurelien Delamotte. 2017. "Increasing the Energy-Efficiency of Induction Machines by the Use of Grain Oriented Magnetic Materials and Die-Casting Copper Squirrel Cage in the Rotor." In *2017 IEEE International Electric Machines and Drives Conference (IEMDC)*, 1–6. Miami, FL, USA: IEEE. https://doi.org/10.1109/IEMDC.2017.8002251.

Ozcelik, Nezih Gokhan, Ugur Emre Dogru, Murat Imeryuz, and Lale T. Ergene. 2019. "Synchronous Reluctance Motor vs. Induction Motor at Low-Power Industrial Applications: Design and Comparison." *Energies* 12 (11): 2190. https://doi.org/10.3390/en12112190.

Pellegrino, Gianmario, Thomas M. Jahns, Nicola Bianchi, Wen Soong, and Francesco Cupertino. 2016. *The Rediscovery of Synchronous Reluctance and Ferrite Permanent Magnet Motors*. SpringerBriefs in Electrical and Computer Engineering. Cham: Springer International Publishing. https://doi.org/10.1007/978-3-319-32202-5.

Pereira, Manuel, and Rui Esteves Araújo. 2019. "Analysis and Design of a Speed Controller for Switched Reluctance Motor Drive." *U.Porto Journal of Engineering* 5 (1): 46–58. https://doi.org/10.24840/2183-6493_005.001_0004.

Sang-Ho Lee, Soon-O Kwon, Jeong-Jong Lee, and Jung-Pyo Hong. 2009. "Characteristic Analysis of Claw-Pole Machine Using Improved Equivalent Magnetic Circuit." *IEEE Transactions on Magnetics* 45 (10): 4570–73. https://doi.org/10.1109/TMAG.2009.2023429.

Selvaraj, D.E., L.J. Ganesan, and S. Jeyadevi. 2013. "Energy Efficient Single Phase Induction Motor." In *Fifth International Conference on Advances in Recent Technologies in Communication and Computing (ARTCom 2013)*, 436–39. Bangalore, India: Institution of Engineering and Technology. https://doi.org/10.1049/cp.2013.2222.

Verucchi, Carlos, Cristian Ruschetti, Esteban Giraldo, Guillermo Bossio, and José Bossio. 2017. "Efficiency Optimization in Small Induction Motors Using Magnetic Slot Wedges." *Electric Power Systems Research* 152 (November): 1–8. https://doi.org/10.1016/j.epsr.2017.06.012.

Vijayakumar, K., R. Karthikeyan, S. Paramasivam, R. Arumugam, and K.N. Srinivas. 2008. "Switched Reluctance Motor Modeling, Design, Simulation, and Analysis: A Comprehensive Review." *IEEE Transactions on Magnetics* 44 (12): 4605–17. https://doi.org/10.1109/TMAG.2008.2003334.

Xiuhe Wang, Chang, Rong Zhang, Renyuan Tang, and Hahn Song-Yop. 2006. "Performance Analysis of Single-Phase Induction Motor Based on Voltage Source Complex Finite-Element Analysis." *IEEE Transactions on Magnetics* 42 (4): 587–90. https://doi.org/10.1109/TMAG.2006.871454.

Yetgin, Asim Gökhan, and Mustafa Turan. 2014. "Efficiency Optimization of Slitted–Core Induction Motor." *Journal of Electrical Engineering* 65 (1): 60–64. https://doi.org/10.2478/jee-2014-0009.

Yoneoka, Yasuei, and Kan Akatsu. 2011. "An Optimized Design of High-Efficiency Switched Reluctance Motor with Single-Phase Input Operation." In *2011 International Conference on Electrical Machines and Systems*, 1–6. Beijing, China: IEEE. https://doi.org/10.1109/ICEMS.2011.6073342.

Zhang, Qian, Huijuan Liu, Zhenyang Zhang, and Tengfei Song. 2018. "A Cast Copper Rotor Induction Motor for Small Commercial EV Traction: Electromagnetic Design, Analysis, and Experimental Tests." *CES Transactions on Electrical Machines and Systems* 2 (4): 417–24. https://doi.org/10.30941/CESTEMS.2018.00053.